Hybrid SPAD/PD Receiver for Reliable Free-Space Optical Communication

Received 17 August 2020; accepted 3 September 2020. Date of publication 9 September 2020; date of current version 25 September 2020.

Digital Object Identifier 10.1109/OJCOMS.2020.3023009

Hybrid SPAD/PD Receiver for Reliable Free-Space Optical Communication

SHENJIE HUANG (Member, IEEE), AND MAJID SAFARI (Member, IEEE)

(Invited Paper)

School of Engineering, University of Edinburgh, Edinburgh EH9 3JL, U.K.

CORRESPONDING AUTHOR: S. HUANG (e-mail: shenjie.huang@ed.ac.uk)

This work was supported by Engineering and Physical Sciences Research Council (EPSRC) under Grant EP/R023123/1 (ARROW).

ABSTRACT Free-space optical (FSO) communication provides wireless optical connectivity with high data rates and low-cost implementation; however, its performance is strongly influenced by the power attenuation due to the infrequent adverse weather conditions. This article proposes a novel highly sensitive dual-mode receiver comprising an array of single-photon avalanche diodes (SPADs) and a PIN photodiode (PD) to enhance the availability of FSO links. In adverse weather conditions, the receiver operates in the SPAD-mode; whereas, in the clear weather conditions, the receiver works in the PD-mode. A hybrid receiver controller is employed in the proposed receiver to adaptively control the switching process based on the received light levels. The adaptive controller also adjusts the incident photon rate of the SPAD array using a variable optical attenuator (VOA) to optimize the performance of the SPAD unit. Our extensive performance analysis illustrates the superior achievable data rates of the proposed receiver under various weather conditions compared to the traditional FSO receivers with either PD or SPAD array.

INDEX TERMS Optical wireless communications, free-space optical communication, optical receivers, single-photon avalanche diode.

I. INTRODUCTION

IN RECENT decades, as the scarcity in the radio frequency spectrum becomes the bottleneck in the development of the wireless communication networks, free-space optical communication (FSO) has attracted significant interest in both industry and scientific community due to its high data rate, excellent security level, and license-free spectrum [1]. The potential applications of FSO include but not limited to inter-building communication and wireless backhaul solution of the future 6G systems. However, before the wide-scale deployment and utilization of FSO systems, some major technical challenges still remain to be overcome, e.g., turbulence-induced intensity fluctuation (scintillation), misalignment loss induced by building sway, and link failure in the presence of adverse weather condition.

Both turbulence-induced fluctuation (also known as scintillation) and misalignment have been thoroughly investigated in the literature. To mitigate the degradation of intensity fluctuation, numerous effective techniques have been proposed such as spatial diversity [2] and multi-hop relaying [3]. For the misalignment loss, beamwidth optimization [4] or adaptive tracking systems [5], [6] can be employed. Different from the above impacts, the signal attenuations introduced by adverse weather conditions, e.g., fog and haze, are fairly static both in time and space and could be up to several hundred of dB/km [7]. To increase the availability of FSO links during adverse weather conditions, the so-called *hybrid RF/FSO links* have been proposed in which an additional RF link is employed to support the FSO link and maintain the connectivity [8]–[10]. Although adding RF links can effectively improve the availability, it inevitably increases the complexity and the cost of the links.

Linear photodiode (PD) is commonly used in commercial FSO links due to its low cost and implementation complexity [1]. However, the sensitivity of linear PD, especially PIN PD, is strongly limited by the thermal noise. In order to improve the receiver sensitivity, PD can be biased above the breakdown voltage to be operated in Geiger mode as a single-photon avalanche diode (SPAD). Due to its high sensitivity compared to the traditional PIN

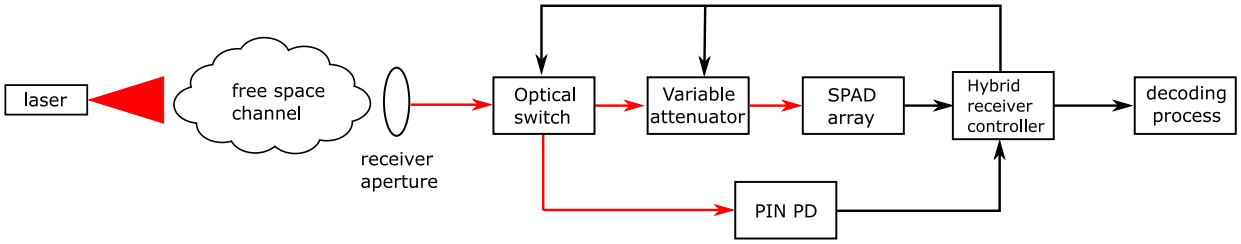

FIGURE 1. The schematic diagram of the proposed system.

PD and avalanche photodiode (APD), SPAD-based receiver can be used to effectively reduce the gap to the quantum limit [11]. Recently, SPAD has attracted particular attention in the context of both visible light communication (VLC) [12], [13] and underwater wireless optical communications (UWOC) [14], [15]. However, the achievable sensitivity of the current SPAD receivers is still limited by several non-ideal factors, e.g., dead time, afterpulsing, fill factor and crosstalk. In particular, dead time refers to the inactive period happens following the avalanche caused by each photon detection when the SPAD is getting quenched. There are two typical types of quenching circuits in SPAD receivers, i.e., active quenching (AQ) and passive quenching (PQ). The dead time of the former type of SPAD is constant, whereas for the latter the photons arriving during the dead time can extend its duration [16]. Dead time can significantly degrade the performance of the SPAD-based receiver when the incident light intensity is relatively high because of the non-linear distortion caused by the SPAD saturation [15], [17].

Inspired by the characteristics of the SPAD and linear PD, we propose to design a dual-mode hybrid receiver contains both PIN PD and SPAD array detectors. Such hybrid receiver can effectively improve the availability of the FSO link for a wide range of weather conditions. In adverse weather conditions, the received light power is relatively weak and the receiver would operate in the SPAD-mode due to the high sensitivity of the SPAD array. However, in the clear weather condition, the received optical power is relatively high and the receiver would in turn switch to the PD-mode. Since in this scenario, the SPAD array suffers from significant non-linear distortion; whereas the PD is with high signal-to-noise ratio (SNR) and can achieve reliable communication. Recently, the design of optical sensors with both PD and SPAD modes have been proposed mainly for imaging applications [18]–[20]. Particularly, in [19] an array of 64 pixels is presented in which the linear and single-photon operations are combined at the pixel level to improve the dynamic range. Each individual pixel can alternatively switch between these modes according to the applied voltage signal; however, the reported bandwidth and photon detection probability (PDP) is quite limited and the complex circuit design also results in a low fill factor. As a result, it is not suitable to be applied in the high-speed sensitive FSO links. To the best of the authors' knowledge, the proposed receiver here is the first time a hybrid SPAD/PD receiver is designed from the communication point of view. The effectiveness of the proposed dual-mode receiver in the improvement of the achievable data rate against the traditional FSO receivers with either PD or SPAD is confirmed through the numerical results.

The rest of this article is organized as follows. The proposed hybrid receiver and the received signal and background power in FSO systems are discussed in Section II. Section III presents the implementation of the proposed hybrid receiver. The numerical results and discussion are presented in Section IV. Finally, we conclude this article in Section V.

II. SYSTEM MODEL

A. PROPOSED HYBRID RECEIVER

Fig. 1 shows the schematic of the proposed system. A laser is employed at the transmitter and the modulated optical signal is transmitted through the atmosphere which introduces both atmospheric intensity fluctuation and weather attenuation loss to the signal received by the receiver aperture. The proposed receiver involves both a PQ-based SPAD-array which is with high sensitivity and a cost-effective PIN PD which is commonly employed in commercial FSO links. Note that compared to AQ SPAD, PQ SPAD benefits from simpler circuit design and higher photon detection efficiency (PDE), hence is widely employed in the commercial SPAD receivers [21]. The proposed receiver can operate in either PIN PD mode or SPAD mode with the help of the binary optical switch. The received optical power (both signal and background power) is monitored by the hybrid receiver controller. When the received power experiences significant change due to the change of the scintillation (on the order of milliseconds [5]) and/or weather condition (usually on the order of hours [10]), the optimal operation mode which achieves the better performance, e.g., higher achievable data rate, is determined by the controller (as discussed later in Section III) and a control signal is sent to the optical switch to realize the mode switching. Generally, when the received optical power is high, PD-mode is selected and optical switch guides the whole received light to the PIN PD; otherwise, the received light is switched to the high-sensitivity SPAD detector. Many different techniques can be employed to realize the fast optical switching [22]. One of the common approach is using the micro-electro-mechanical systems (MEMS) in which the angle of the micro-mirrors

can be adjusted through the supplied electrical currents to deflect an optical signal to the desired receiver [23]. After the mode switching is finished, based on the current receiver operation mode, the controller selects either the electrical output of the SPAD array or PD detector to the following decoding process.

Because of the very limited dynamic range of the SPAD-array receiver (determined by the number of pixels and the dead time), it can be easily saturated when the received optical power increases beyond a specific level. Further increase in the optical power results in the significant performance degradation for PQ SPAD detector employed here. However, due to the high sensitivity of the SPAD detector compared to the PD, it is highly likely that such a power level is still not high enough for the PD to achieve reliable communication. As a result, there is a gap between the operational ranges of the SPAD and PIN PD (as demonstrated in Section IV). To address this issue, in the proposed hybrid receiver, a variable optical attenuator (VOA) [24]–[26] with its transmittance adaptively controlled by the receiver controller is employed to attenuate the incident light to SPAD array when necessary. By proper adjusting the VOA transmittance, the SPAD detector can keep operating in a higher received optical power regime. As a result, the gap of the operation regimes between the PD and SPAD array can be bridged and the proposed receiver is able to achieved high data rates in a wide range of the received optical power.

Although this work focuses on the application of the proposed receiver in FSO systems, it is worth emphasizing that the proposed receiver also has potential applications in other OWC systems such as indoor VLC and UWOC systems. Due to the blockage or dimming in VLC and strong absorption and scattering in UWOC, the received signal power could be very weak. The proposed receiver is advantageous in such scenario as it can switch to the high-sensitive SPAD mode. On the other hand, in other scenarios where the received power is relatively high, the receiver can instead operate in the PIN PD mode.

B. RECEIVED SIGNAL POWER

In the considered FSO system, assuming that the pointing error is negligible due to a relatively large received beam spot and/or the use of a tracking system, the received optical signal is mainly influenced by three effects, i.e., geometric loss induced by diffraction h_g, turbulence-induced intensity fluctuation h_f, and weather-induced attenuation h_a. Denoting the transmitted optical power as P_T, the instantaneous received power can be expressed as

$$P_R = h_g h_f h_a P_T. \tag{1}$$

The geometric loss h_g can be expressed as [9]

$$h_g = \left[\mathrm{erf}\left(\frac{\sqrt{\pi}d}{2\sqrt{2}\phi L}\right)\right]^2, \tag{2}$$

where d denotes the diameter of the receiver aperture, ϕ is the beam divergence angle at the transmitter, and L refers to the link distance. The weather attenuation h_a can be expressed based on the Beer-Lambert law as

$$h_a = e^{-\kappa L}, \tag{3}$$

where κ is a visibility-dependent attenuation coefficient given by [27]

$$\kappa = \frac{3.91}{V}\left(\frac{\lambda_{\mathrm{op}}}{550\times 10^{-9}}\right)^{-\varrho}, \tag{4}$$

V refers to the visibility in km, λ_{op} is the optical wavelength and the coefficient ϱ is given by

$$\varrho = \begin{cases} 1.6, & V \geq 50\,\mathrm{km}, \\ 1.3, & 6 \leq V < 50\,\mathrm{km}, \\ 0.16V + 0.34, & 1 \leq V < 6\,\mathrm{km}, \\ V - 0.5, & 0.5 \leq V < 1\,\mathrm{km}, \\ 0, & V < 0.5\,\mathrm{km}. \end{cases} \tag{5}$$

Note that the above model of the fog attenuation is widely used in the literature; however, there are also some other models which are more accurate under some specific wavelength regimes [28] and could also be employed in the proposed system.

Numerous models can be used to model the turbulence-induced intensity fluctuation h_f, e.g., log-normal distribution and Gamma-Gamma distribution. To ensure that a wide range of turbulence conditions can be accurately described, the Gamma-Gamma distribution is employed here as given by [29]

$$f_{h_f}(x) = \frac{2(\alpha\beta)^{(\alpha+\beta)/2}}{\Gamma(\alpha)\Gamma(\beta)} x^{(\alpha+\beta)/2-1} K_{\alpha-\beta}\left(2\sqrt{\alpha\beta x}\right), \tag{6}$$

where $\Gamma(\cdot)$ is the Gamma function, $K_p(\cdot)$ is the modified Bessel function of the second kind, and the parameter α and β are given by

$$\alpha = \left[\exp\left(\frac{0.49\chi^2}{\left(1+0.18\vartheta^2+0.56\chi^{12/5}\right)^{7/6}}\right) - 1\right]^{-1}, \tag{7}$$

$$\beta = \left[\exp\left(\frac{0.51\chi^2\left(1+0.69\chi^{12/5}\right)^{-5/6}}{\left(1+0.9\vartheta^2+0.62\vartheta^2\chi^{12/5}\right)^{5/6}}\right) - 1\right]^{-1}, \tag{8}$$

respectively, with $\chi^2 = 0.5C_n^2 k^{7/6} L^{11/6}$, $\vartheta^2 = kd^2/4L$ and $k = 2\pi/\lambda_{\mathrm{op}}$. The parameter C_n^2 refers to the turbulence refraction structure parameter.

The coherence time of h_f is shorter than that of the weather attenuation h_a, thus the coherence time of the received power P_R is mainly determined by h_f. In the proposed receiver, as long as P_R experiences significant change due to the change of h_a and/or h_f, the receiver mode switching process is triggered.

C. RECEIVED BACKGROUND POWER

In FSO communication, the received background power can greatly influence the receiver performance. Adverse weather conditions, e.g., fog, can change both received signal and

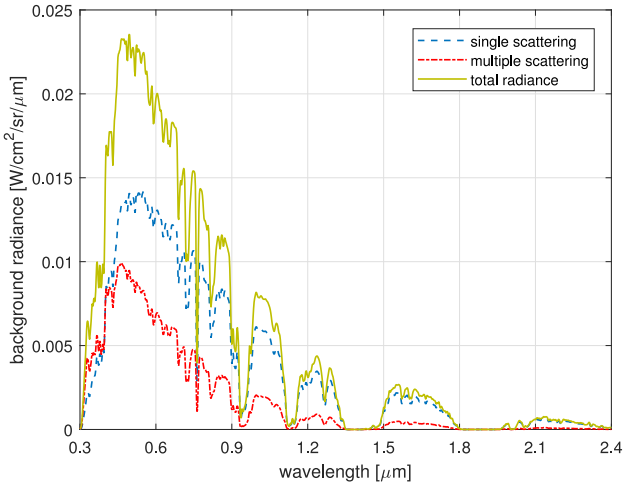

FIGURE 2. A example of the spectral background radiance in clear weather condition. Take the receiver as the reference location. The LOS is with zenith angle of 90° and the relative solar zenith angle is 45°.

background power. The signal power attenuation in fog conditions has been thoroughly investigated in the literature [27], [28]; however, the weather dependency of the received background power is not well discussed. In this work, we are going to fill this research gap with the help of the software MODTRAN which can compute the atmospheric radiance over the ultraviolet through long wavelength infrared spectral regime [30].

Practical FSO systems are usually designed with proper line-of-sight (LOS) angles and narrow receiver field-of-views (FOVs) to avoid receiving the direct sunlight. Therefore, the main background noise source is the sunlight scattered in the atmosphere (or the diffused sky radiance). The received background power can hence be written as [31]

$$P_b = \pi^2 R_B \Delta\lambda_{\text{op}} d^2 \sin^2\left(\frac{\theta_{\text{FOV}}}{4}\right). \tag{9}$$

where R_B is the spectral radiance of the scattered sunlight (W/cm^2·sr·μm), $\Delta\lambda_{\text{op}}$ is the bandwidth of the receiver optical filter, θ_{FOV} is the receiver FOV angle. The spectral radiance R_B which can be simulated through MODTRAN is determined by both visibility and solar position relative to the link LOS. An example of the simulated spectral background radiance under clear weather condition is presented in Fig. 2. The total background radiance R_B mainly contains radiance caused by single and multiple scattering. As illustrated in Section IV, lower visibility can result in lower single scattering induced background radiance; whereas this is not the case for multiple scattering induced radiance. Therefore, lower visibility might not always lead to lower background radiance or equivalently lower received background power. This is different from the effects of the fog events to the received signal power. Later in Section IV, in order to accurately evaluate the performance of the proposed receiver under various visibilities, for each visibility level the radiance is firstly simulated by MODTRAN based on which the corresponding received background power P_b can be calculated through (9).

III. HYBRID RECEIVER IMPLEMENTATION

Since both PIN PD and SPAD array detector are employed in the proposed hybrid receiver, in this section the achievable data rate of each receiver is firstly derived. Later, the implementation of the hybrid receiver is presented.

A. PERFORMANCE OF THE PIN PD

When the proposed receiver operates in PD mode, the received light is switched to the PIN PD and the electrical SNR can be expressed as [32], [33]

$$\gamma_{PD} = \frac{2P_R^2\Phi^2}{2qB\Phi(P_R + P_b) + \frac{4\kappa T^o B}{R_L}}, \tag{10}$$

where q refers to the electron charge, Φ denotes the photodiode responsivity, P_b is the received background light power, κ is the Boltzmann's constant, T^o is the load-resistor temperature in Kelvin, R_L is the load resistance and B denotes the electrical bandwidth. The first term in the denominator of (10) refers to the shot noise and the second term represents the thermal noise. The thermal noise is the dominant noise component. In this work, the uncoded equiprobable on-off keying (OOK) modulation is employed as the modulation scheme, although the proposed idea can also be extended to systems with other higher order modulation schemes. In addition, the transmitted signal is assumed to be with an ideal infinite extinction ratio so that the received power for bit '0' is simply P_b. The BER of the PD detector can be expressed as

$$BER_{PD} = Q\left(\sqrt{\frac{1}{2}\gamma_{PD}}\right), \tag{11}$$

where $Q(\cdot)$ refers to the Q-function.

Assuming a BER threshold of $P_{e,th}$, for PD detector to achieve this BER target,

$$Q\left(\sqrt{\frac{1}{2}\gamma_{PD}}\right) \le P_{e,th}, \tag{12}$$

should be satisfied. Substituting the SNR of the PD (10) into (12) and after some mathematical manipulations, the maximum achievable data rate for PD detector as a function of P_R and P_b can be expressed as

$$R_{\text{PD}}^{\max}(P_R, P_b) = \frac{P_R^2\Phi^2}{\left[q\Phi(P_R + P_b) + \frac{2\kappa T^o}{R_L}\right]\left[Q^{-1}(P_{e,th})\right]^2}, \tag{13}$$

where $Q^{-1}(\cdot)$ denotes the inverse Q-function.

B. PERFORMANCE OF THE SPAD ARRAY

Different from the traditional photodetectors, the SPAD detectors suffer from the dead time in which the SPAD is

inactive after the avalanche caused by each photon detection. The photon transfer function of PQ SPAD is given by [34]

$$\lambda_D = \lambda \exp(-\lambda \tau_d), \tag{14}$$

where λ is the received photon rate, τ_d is the dead time and λ_D refers to the detected photon rate. Based on (14), one can observe that due to the paralysis property of the PQ SPAD, with the increase of received photon rate, the detected photon rate firstly increases and then decreases. The received photon rate which gives the highest detected photon rate is $\lambda_{\max} = 1/\tau_d$ and the corresponding detected photon rate is $\lambda_{D,\max} = 1/e\tau_d$. The non-linear distortion shown in the photon transfer function (14) would significantly influence the performance of the SPAD-based receivers [35]. To involve the non-linear distortion into the system analysis, it is commonly assumed that the detected photon count of SPAD array is Poisson distributed with effective photon rate given in (14) which is an accurate approximation in low photon arrival rate regimes as illustrated in [15], [36]. For large array sizes, the overall photon counts can be further approximated as Gaussian [14]. In the following discussion, we thus employ the Gaussian approximation for the detected photon counts.

Considering a received signal power P_R and background light power P_b, for a SPAD array detector with N pixels, the received photon rate for each pixel when bit '0' and bit '1' are sent can be expressed as

$$\begin{aligned} \lambda_0(\xi) &= \frac{\xi \Upsilon_{\text{PDE}} P_b}{Nh\nu}, \\ \lambda_1(\xi) &= \frac{\xi \Upsilon_{\text{PDE}} (2P_R + P_b)}{Nh\nu}, \end{aligned} \tag{15}$$

where ξ denotes the transmittance of the employed VOA, Υ_{PDE} is the PDE of the SPAD, h refers to the Planck constant, and ν is the light frequency. Note that the photon rates given in (15) are written as functions of the adjustable transmittance ξ. In this work, the dead time is considered to be the main non-ideal effect of the SPAD receiver and the other effects, e.g., crosstalk and dark count, are ignored for simplicity. According to the effective photon rate (14), the average photon counts for bit '0' and bit '1' during the symbol duration T_s are given by

$$\begin{aligned} u_0(\xi) &= N\lambda_0(\xi) T_s e^{-\lambda_0(\xi)\tau_d}, \\ u_1(\xi) &= N\lambda_1(\xi) T_s e^{-\lambda_1(\xi)\tau_d}. \end{aligned} \tag{16}$$

Assuming Gaussian distribution for detected photon counts of bit '0' (bit '1') with mean and variance equal to u_0 (u_1), the BER can be expressed as [12], [37]

$$BER_{\text{SPAD}} = Q[\zeta(\xi)], \tag{17}$$

where

$$\zeta(\xi) = \frac{u_1(\xi) - u_0(\xi)}{\sqrt{u_1(\xi)} + \sqrt{u_0(\xi)}} = \sqrt{u_1(\xi)} - \sqrt{u_0(\xi)}. \tag{18}$$

In the proposed hybrid receiver, the controller should adjust the ξ so that the SPAD array can operate at its best. The optimal ξ minimizing the BER_{SPAD} is equivalent to the one maximizing the $\zeta(\xi)$ which is given by the following Proposition.

Proposition 1: The optimal ξ which minimizes the BER_{SPAD} can be expressed as

$$\xi^*(P_R, P_b) = \min\left[\frac{Nh\nu\, y_{\text{root},1}}{\Upsilon_{\text{PDE}}\, \tau_d P_R}, 1\right] \tag{19}$$

where $y_{\text{root},1}$ denotes the single positive root of the non-linear equation

$$\frac{P_b}{P_R} y - 1 = \frac{2y}{\sqrt{\frac{P_b}{2P_R+P_b}} e^y - 1}, \tag{20}$$

in the regime $y \in (0, \ln\sqrt{\frac{2P_R+P_b}{P_b}})$.

Proof: The first derivative of $\zeta(\xi)$ with respect to ξ can be expressed as

$$\begin{aligned} \mathcal{D}(\xi) = \frac{\sqrt{u_1(\xi)}}{\xi}\Bigg[\frac{1}{2}\left(1 - \sqrt{\frac{u_0(\xi)}{u_1(\xi)}}\right)\left(1 - \frac{\xi \Upsilon_{\text{PDE}} \tau_d P_b}{Nh\nu}\right) \\ - \frac{\xi \Upsilon_{\text{PDE}} \tau_d P_R}{Nh\nu}\Bigg]. \end{aligned} \tag{21}$$

By substituting $y = \xi \Upsilon_{\text{PDE}} \tau_d P_R / Nh\nu$ and

$$\frac{u_0(\xi)}{u_1(\xi)} = \frac{P_b}{2P_R + P_b} e^{2y}, \tag{22}$$

into (21), it can be simplified as

$$\begin{aligned} \mathcal{D}(y) = \frac{A e^{-\frac{(2P_R+P_b)}{2P_R} y}}{\sqrt{y}} \\ \times \left[\frac{1}{2}\left(1 - \sqrt{\frac{P_b}{2P_R + P_b}} e^y\right)\left(1 - \frac{P_b}{P_R} y\right) - y\right], \end{aligned} \tag{23}$$

where the constant

$$A = \frac{\Upsilon_{\text{PDE}} \sqrt{\tau_d P_R (2P_R + P_b) T_s}}{\sqrt{N} h\nu}. \tag{24}$$

Letting the first order derivative (23) equal to zero one can get the non-linear equation (20). Denoting $\mathcal{T}_1(y) = \frac{P_b}{P_R} y - 1$, it can be easily shown that $\mathcal{T}_1(y)$ is a monotonically increasing function for $y \geq 0$ with $\mathcal{T}_1 = -1$ at $y = 0$ and $\mathcal{T}_1 \to +\infty$ at $y \to +\infty$. On the other hand, denote the right hand side of (20) as

$$\mathcal{T}_2(y) = \frac{2y}{\sqrt{\frac{P_b}{2P_R+P_b}} e^y - 1}, \tag{25}$$

we can show that in the regime $y \in [0, \ln\sqrt{\frac{2P_R+P_b}{P_b}})$, $\mathcal{T}_2$ is a decreasing function with $\mathcal{T}_2 = 0$ at $y = 0$ and $\mathcal{T}_2 \to -\infty$ as y approaches $\ln\sqrt{\frac{2P_R+P_b}{P_b}}$ from the left. In addition, in the regime $y \in (\ln\sqrt{\frac{2P_R+P_b}{P_b}}, +\infty)$, $\mathcal{T}_2$ is also a decreasing function but with $\mathcal{T}_2 \to +\infty$ when y approaches to $\ln\sqrt{\frac{2P_R+P_b}{P_b}}$ from the right and $\mathcal{T}_2 \to 0$ when $y \to +\infty$. Based on the characteristics of the functions $\mathcal{T}_1$ and $\mathcal{T}_2$, it can be proved that there are two roots for the equation (20), denoted as

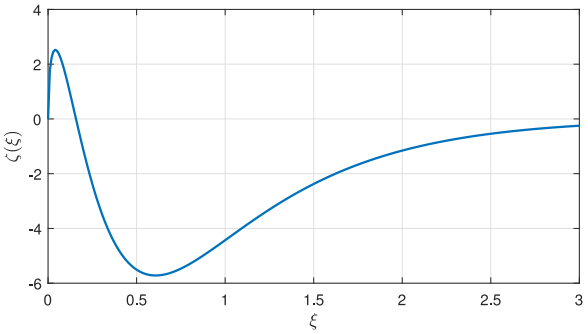

FIGURE 3. An example of the relationship between $\zeta(\xi)$ and ξ.

$y_{\text{root},1}$ and $y_{\text{root},2}$, which satisfy $y_{\text{root},1} \in (0, \ln\sqrt{\frac{2P_R+P_b}{P_b}})$ and $y_{\text{root},2} \in (\ln\sqrt{\frac{2P_R+P_b}{P_b}}, +\infty)$, respectively. Both of these two roots can be found through the bisection method. Finally, since $\mathcal{D}(y \to 0) = +\infty$ and $\mathcal{D}(y = \ln\sqrt{\frac{2P_R+P_b}{P_b}}) < 0$, $y_{\text{root},1}$ is a local maximum. In addition, due to the fact that $\mathcal{D}(y \to +\infty) > 0$, $y_{\text{root},2}$ is a local minimum.

From the above discussion it is concluded that with the increase of ξ, $\zeta(\xi)$ firstly increases when $\xi \in [0, y_{\text{root},1}Nh\nu/\Upsilon_{\text{PDE}}\tau_d P_R]$, then $\zeta(\xi)$ decreases when $\xi \in [y_{\text{root},1}Nh\nu/\Upsilon_{\text{PDE}}\tau_d P_R, y_{\text{root},2}Nh\nu/\Upsilon_{\text{PDE}}\tau_d P_R]$, and finally with further increase of ξ it increases again and gradually approaches 0. An example of the relationship between $\zeta(\xi)$ and ξ is shown in Fig. 3. Considering that the transmittance of the VOA is limited up to 1, the optimal ξ which minimizes the BER, denoted as ξ^*, can hence be written as (19). ■

Solving the non-linear equation (20) can inevitably increase the complexity of the design receiver. If one cannot afford the computational complexity, a look-up table of the optimal ξ under various P_R and P_b could be calculated and pre-saved at the receiver. In the communication, the transmittance of VOA can then be selected optimally by using the table.

To further simplify the receiver design, in this work, we also provide a sub-optimal analytical solution for the selection of ξ which is asymptotically optimal when the background power is small. When P_b is negligible, (17) can be rewritten as

$$BER_{\text{SPAD}} \approx Q\left(\sqrt{N\lambda_1(\xi)T_s e^{-\lambda_1(\xi)\tau_d}}\right). \tag{26}$$

The optimal ξ minimizing BER_{SPAD} can be expressed as

$$\xi^*(P_R, P_b) = \min\left[\frac{Nh\nu}{\tau_d\Upsilon_{\text{PDE}}(2P_R+P_b)}, 1\right]. \tag{27}$$

By substituting (27) into (15), one can get $\lambda_1(\xi^*) = 1/\tau_d$ when received power is high. For PQ SPAD, this incident photon rate is the one resulting in the highest detected photon rate, hence the physical meaning of the sub-optimal transmittance is simply limiting the peak incident photon rate for the SPAD array to be fixed at this value.

Algorithm 1 Algorithm for the Hybrid Receiver Controller

```
keep estimating P_R and P_b.
while P_R and/or P_b have significant change do
    if R_SPAD^max < R_PD^max then
        switch to PD and decode the received signal.
    else
        adjust the transmittance of VOA to ξ*.
        switch to SPAD array and decode the received signal.
    end if
end while
```

By substituting the determined transmittance of the VOA (19) or (27) into (17) and considering a BER target of $P_{e,th}$, after some mathematical manipulations, the maximum achievable data rate of the SPAD array can be written as

$$R_{\text{SPAD}}^{\max}(P_R, P_b) = \left[\frac{\sqrt{N\lambda_1(\xi^*)e^{-\lambda_1(\xi^*)\tau_d}} - \sqrt{N\lambda_0(\xi^*)e^{-\lambda_0(\xi^*)\tau_d}}}{Q^{-1}(P_{e,th})}\right]^2. \tag{28}$$

Note that (28) requires $\xi^* < Nh\nu\ln\frac{2P_R+P_b}{P_b}/2\tau_d\Upsilon_{\text{PDE}}P_R$ and both derived VOA transmittance values (19) and (27) satisfy this condition.

C. IMPLEMENTATION OF THE HYBRID RECEIVER

The key component of the proposed hybrid receiver shown in Fig. 1 is the receiver controller. When the received signal and background power experience significant change due to the scintillation and/or weather change, the controller calculates the maximum achievable data rate for PIN PD based on (13). Meanwhile, the optimal transmittance of the VOA is calculated based on (19) or (27) and the corresponding maximum achievable data rate of the SPAD array is calculated using (28). By comparing the maximum achievable data rates of the SPAD array and PD, the best operation mode can be determined. The controller then sends a control signal to the optical switch to realize the mode switching. If the SPAD array can achieve higher data rate and thus the SPAD mode is selected, the controller should also send a control signal to VOA to adaptively adjust its transmittance to the desired level. When all of the above steps are finished, the controller feeds the selected electrical signal to the following decoding process. An algorithm showing how the hybrid receiver controller works is presented in Algorithm 1. Although this work employs the achievable data rate as the performance metric to determine the operation mode, the proposed receiver can also be designed based on other metrics, e.g., BER performance.

It is worth noting that when applied to FSO systems, the proposed receiver is more likely to be operated in the high-sensitive SPAD mode in adverse weather conditions, e.g., fog and haze, where the received signal power is significantly attenuated. Although adverse weather conditions are usually infrequent [8], considering the high availability requirement of FSO links, it is crucial to keep the link connectivity

TABLE 1. The parameter setting [9], [21], [38], [39].

Symbol	Definition	Value
d	Receiver aperture diameter	10 cm
L	Distance between the source and destination	$[500, 1000]$ m
ϕ	Laser divergence angle	2 mrad
C_n^2	Refraction structure index	5×10^{-15} m$^{-2/3}$
λ_{op}	Laser wavelength	785 nm
P_T	Transmitted power	20 mW
$P_{e,th}$	the BER target	10^{-3}
H	Height of the transceiver	20 m
$\Delta\lambda_{\text{op}}$	Bandwidth of the receiver optical filter	20 nm
θ_{FOV}	Receiver FOV angle	3 mrad
PD detector		
Φ	Responsivity @ $\lambda_{\text{op}} = 785$ nm	0.50 A/W
R_L	Load resistance	50 Ω
T^o	Load-Resistor temperature	297 K
SPAD array detector		
N	Number of SPADs in array	2048
τ_d	SPAD dead time	10 ns
Υ_{PDE}	Photon detection efficiency @ $\lambda_{\text{op}} = 785$ nm	18%

under such conditions. The proposed hybrid receiver could be a good solution to this issue.

IV. NUMERICAL RESULTS

In this section, some numerical results are presented. Unless otherwise mentioned, the specifications of the considered FSO is given in Table 1. Note that most of the current commercial FSO links use wavelengths between 780 nm and 1550 nm due to the relatively lower atmospheric attenuation and the readily available off-the-shelf components [1], [40]. Considering that both PD and SPAD detectors with relatively high detection efficiency at 785 nm are commercially available, this wavelength is employed in our simulations [21], [39]. We will firstly focus on the performance improvement by employing the proposed receiver under the given received signal power P_R and background power P_b. Later, the performance of the practical FSO link under various visibilities is investigated by further involving both turbulence-induced fluctuation and weather attenuation into account.

A. PERFORMANCE IMPROVEMENT UNDER GIVEN RECEIVED POWER

Fig. 4 to Fig. 6 plot the achievable data rate versus the received signal power P_R under various background power P_b and a BER target of $P_{e,th} = 10^{-3}$. Four receivers are considered here. The first two refer to the receivers with PIN PD and SPAD array, respectively. The next two refer to the proposed hybrid receivers with the optimal and sub-optimal transmittance of VOA given in (19) and (27), respectively.

For receiver with SPAD array, these figures present that with the increase of P_R the achievable data rate firstly increases and then decreases. This is because for high P_R regime, non-linear distortion caused by the SPAD saturation

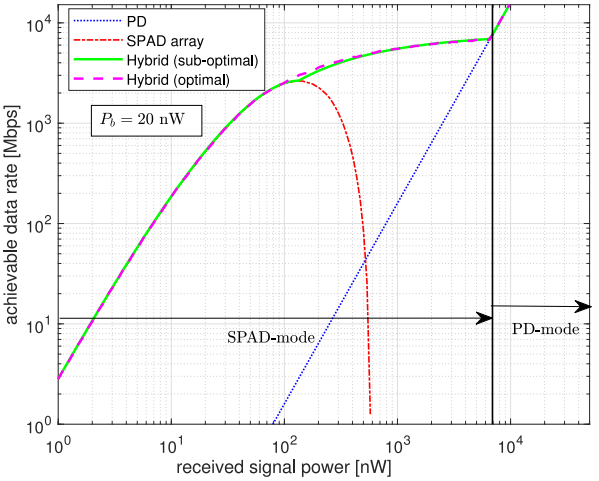

FIGURE 4. The achievable data rate versus the received signal power P_R for considered systems. The background light power is $P_b = 20$ nW.

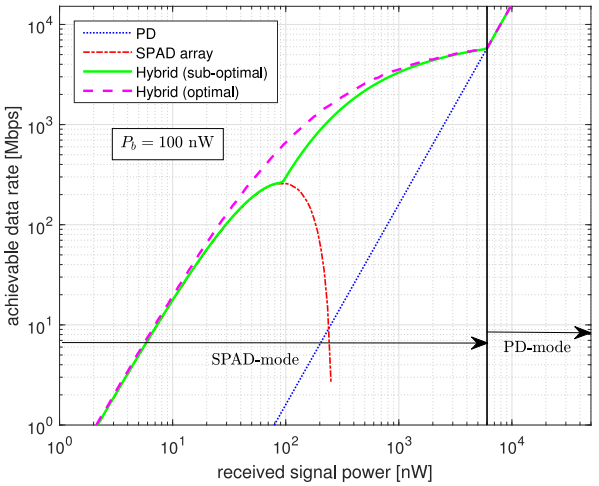

FIGURE 5. The achievable data rate versus the received signal power P_R for considered systems. The background light power is $P_b = 100$ nW.

significantly degrades the performance of the receiver. As shown in Fig. 4, when received background power is weak, gigabits/second data rate can be achieved only when the P_R is beyond 33 nW and below 331 nW. However, with the increase of P_b, the achievable data rate is strongly reduced. For instance, as presented in Fig. 5, when P_b increases to 100 nW, gigabits/second data rate cannot be achieved no matter what signal power is received and the highest achievable data rate is only 273 Mbit/s when $P_R = 90$ nW. On the hand, one can also observe that the effects of the background power to the performance of the system with PIN PD receiver is negligible. This is because thermal noise is the dominant noise factor for the PIN PD. For such receiver to achieve gigabits/second data rate, a received signal power above 2.4 μW (-26 dBm) is required.

Now let's turn to the proposed hybrid receiver. As illustrated from Fig. 4 to Fig. 6, the proposed receiver has two operation modes and when the received power is relatively

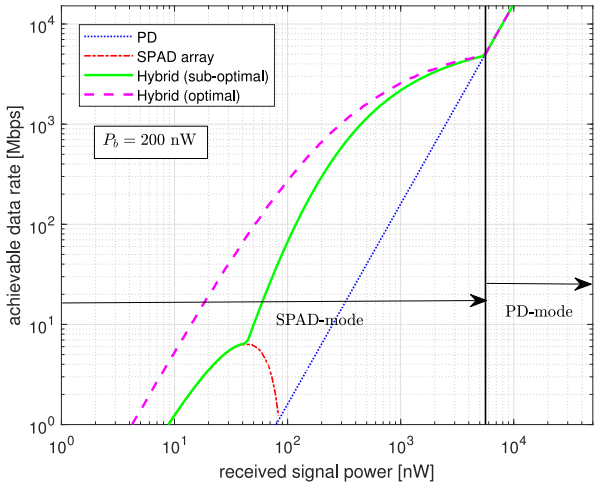

FIGURE 6. The achievable data rate versus the received signal power P_R for considered systems. The background light power is $P_b = 200$ nW.

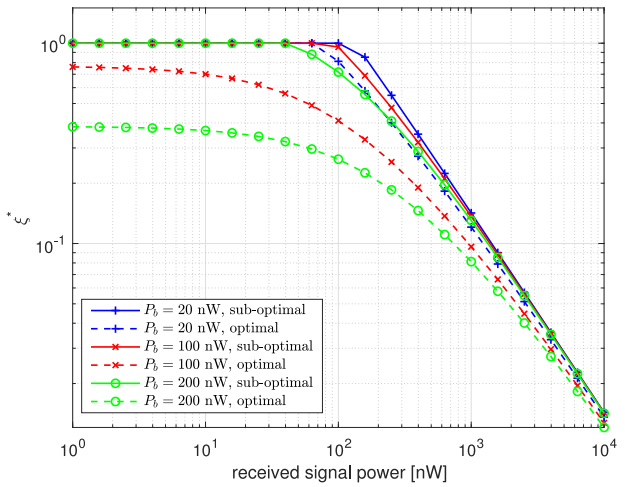

FIGURE 7. The optimal and sub-optimal transmittance of the VOA versus the average received signal power.

small, it operates in SPAD-mode; whereas, when the received power is high, it operates in PD-mode. The main difference between the optimal and sub-optimal hybrid receivers is the selection of the VOA transmittance ξ^* as given in (19) and (27). Fig. 7 shows the calculated transmittance of VOA for these two systems. It demonstrated that for both systems, with the increase of the received signal and background power, the selected transmittance reduces. This is because higher incident light introduces severer SPAD saturation effect and reducing the transmittance can effectively mitigate this effect and improve the performance. In addition, the sub-optimal transmittance is generally higher than the optimal one. As discussed in Section III-B, when background power is negligible, the performance of the sub-optimal design is close to that of the optimal one. This is also illustrated in Fig. 4 where a weak background power is considered. However, with the increase of the background power, the advantage of the optimal design becomes

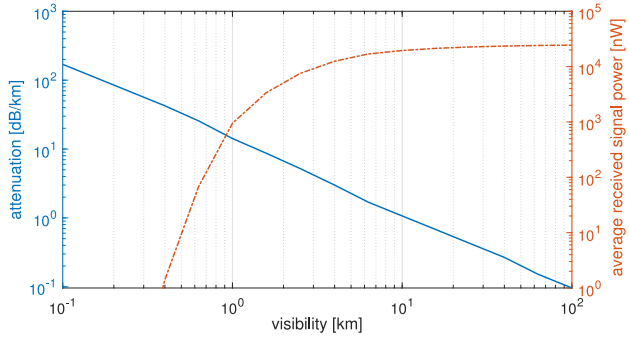

FIGURE 8. The weather attenuation and the average received signal power versus the visibility where $L = 1$ km.

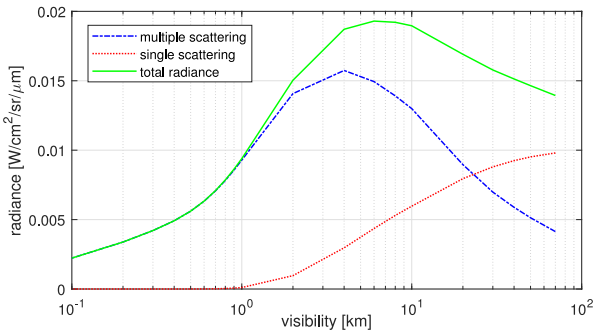

FIGURE 9. The background radiance versus the visibility. Take the receiver as the reference location. The LOS is with zenith angle of 90° and the relative solar zenith angle is 45°.

obvious as presented in Fig. 5 and Fig. 6. For instance, with $P_b = 200$ nW and $P_R = 41$ nW, the sub-optimal design can only achieve a data rate of 6 Mbps which is close to the peak achievable data rate of the SPAD only receiver; whereas, for the receiver with optimal design, the corresponding data rate increases to 70 Mbps.

It is presented from Fig. 4 to Fig. 6 that SPAD array and PD receivers have quite different operation regimes. As a result, a basic combination of the two receivers cannot provide a monotonically increasing performance level as the received signal power increases. By involving the VOA into the system, The proposed hybrid receiver can effectively bridge the gap between the operation regimes of the two detectors realizing the monotonically increasing performance. For instance, for proposed receiver with optimal VOA transmittance, the gigabits/second data rate can always be guaranteed as long as P_R is larger than around 150 nW (-38 dBm) and 300 nW (-35 dBm) when $P_b = 100$ nW and $P_b = 200$ nW, respectively. Invoking the corresponding required power for PIN PD -26 dBm, the sensitivity improvements by using the hybrid receiver are 12 dB and 9 dB, respectively.

B. PERFORMANCE IMPROVEMENT IN PRACTICAL FSO LINKS

Fig. 8 illustrates the weather attenuation in dB/km and the received signal power averaged over the turbulence-induced

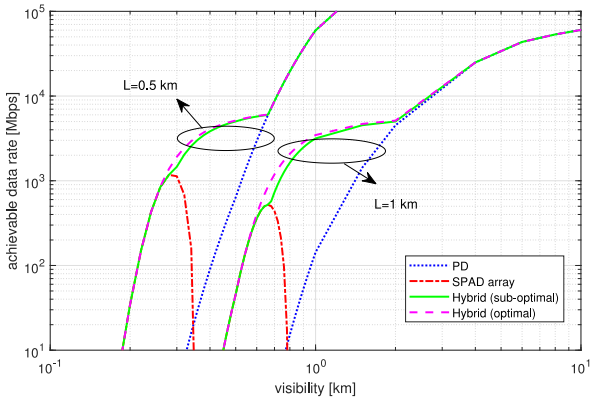

FIGURE 10. The achievable data rate versus the weather visibility under various link distances.

intensity fluctuation, i.e., $\overline{P_R} = h_g h_a P_T$, versus the visibility. Fog events with visibility less than 2 km can introduce great signal attenuation. For instance when visibility $V = 1$ km (light fog), the attenuation is 14.2 dB/km and when visibility reduces to $V = 500$ m (moderate fog), the attenuation increases to 68 dB/km.

The background radiance for the wavelength $\lambda_{\text{op}} = 785$ nm versus the visibility generated by MODTRAN is presented in Fig. 9. One can observe that in clear weather conditions, the background radiance induced by single scattering is the dominant factor. With the decrease of the visibility, the radiance introduced by single scattering monotonically decreases; however, the radiance introduced by multiple scattering firstly increases and then decreases. The reason is that moderate scattering effect can increase the probability of the background light being scattered into the receiver FOV, but extensive scattering effect in turn reduces this probability. The received background power P_b under various visibilities can be achieved by substituting the total radiance R_B into (9).

By using the received signal power and background light radiance demonstrated in Fig. 8 and Fig. 9, respectively, the achievable data rate of the practical FSO link versus the visibility is plotted in Fig. 10. It is shown that for a receiver with PIN PD, in order to achieve 1 Gbps and 100 Mbps data rates, the minimal tolerant visibilities are 1.4 km and 0.96 km, respectively, when the link distance is $L = 1$ km. These visibilities refer to the thin fog conditions. However, the corresponding required visibilities for the proposed hybrid receiver with optimal VOA transmittance reduce to 680 m and 520 m, respectively, which refer to the light fog conditions. Therefore, by using the proposed receiver, the availability can be effectively improved. Note that for the proposed hybrid receiver, with the help of the VOA, the monotonic increase of achievable data rate with the increase of visibility can be observed. Better availability can be achieved for a FSO link with lower distance due to the higher received power gain. For instance, when $L = 500$ m, by using the proposed hybrid receiver, the minimal tolerant visibility for 1 Gbps is only 250 m, hence reliable gigabits/second data rate can be guaranteed even in moderate fog condition. Besides reducing the link distance, the availability can be further improved by employing more expensive narrower bandwidth optical filter at the receiver or increasing the transmitted optical power.

V. CONCLUSION

In this work, a novel hybrid PD/SPAD receiver is proposed to improve the sensitivity of FSO links. The receiver can adaptively operate in either SPAD- or PD-mode depending on the received signal and background light power. In addition, to extend the operation regime of the SPAD array, a VOA is employed to dynamically limit the incident light power of the SPAD array so that it can achieve the best performance. Both optical switch and VOA are controlled by a hybrid receiver controller. A detailed algorithm of the controller is presented. Through extensive numerical results, the effectiveness of the proposed receiver in enhancing the achievable data rate under various visibility conditions is confirmed.

REFERENCES

[1] M. A. Khalighi and M. Uysal, "Survey on free space optical communication: A communication theory perspective," *IEEE Commun. Surveys Tuts.*, vol. 16, no. 4, pp. 2231–2258, 4th Quart., 2014.
[2] M. Safari and S. Hranilovic, "Diversity and multiplexing for near-field atmospheric optical communication," *IEEE Trans. Commun.*, vol. 61, no. 5, pp. 1988–1997, May 2013.
[3] M. Safari, M. M. Rad, and M. Uysal, "Multi-hop relaying over the atmospheric Poisson channel: Outage analysis and optimization," *IEEE Trans. Commun.*, vol. 60, no. 3, pp. 817–829, Mar. 2012.
[4] A. A. Farid and S. Hranilovic, "Outage capacity optimization for free-space optical links with pointing errors," *J. Lightw. Technol.*, vol. 25, no. 7, pp. 1702–1710, Jul. 9, 2007.
[5] S. Bloom, E. Korevaar, J. Schuster, and H. Willebrand, "Understanding the performance of free-space optics," *J. Opt. Netw.*, vol. 2, no. 6, pp. 178–200, Jun. 2003.
[6] S. Huang and M. Safari, "Free-space optical communication impaired by angular fluctuations," *IEEE Trans. Wireless Commun.*, vol. 16, no. 11, pp. 7475–7487, Sep. 2017.
[7] I. I. Kim and E. J. Korevaar, "Availability of free-space optics (FSO) and hybrid FSO/RF systems," in *Proc. Opt. Wireless Commun. IV*, vol. 4530, 2001, pp. 84–95.
[8] S. Huang, V. Shah-Mansouri, and M. Safari, "Game-theoretic spectrum trading in RF relay-assisted free-space optical communications," *IEEE Trans. Wireless Commun.*, vol. 18, no. 10, pp. 4803–4815, Jul. 2019.
[9] V. Jamali, D. S. Michalopoulos, M. Uysal, and R. Schober, "Link allocation for multiuser systems with hybrid RF/FSO backhaul: Delay-limited and delay-tolerant designs," *IEEE Trans. Wireless Commun.*, vol. 15, no. 5, pp. 3281–3295, Jan. 2016.
[10] W. Zhang, S. Hranilovic, and C. Shi, "Soft-switching hybrid FSO/RF links using short-length raptor codes: Design and implementation," *IEEE J. Sel. Areas Commun.*, vol. 27, no. 9, pp. 1698–1708, Dec. 2009.
[11] H. Zimmermann, "APD and SPAD receivers: Invited paper," in *Proc. 15th Int. Conf. Telecommun. (ConTEL)*, 2019, pp. 1–5.
[12] L. Zhang *et al.*, "A comparison of APD- and SPAD-based receivers for visible light communications," *J. Lightw. Technol.*, vol. 36, no. 12, pp. 2435–2442, Jun. 28, 2018.
[13] D. Chitnis *et al.*, "A 200 Mb/s VLC demonstration with a spad based receiver," in *Proc. IEEE Summer Topicals Meeting Series (SUM)*, 2015, pp. 226–227.
[14] M. Khalighi, T. Hamza, S. Bourennane, P. Lon, and J. Opderbecke, "Underwater wireless optical communications using silicon photomultipliers," *IEEE Photon. J.*, vol. 9, no. 4, pp. 1–10, Jul. 2017.

[15] M. A. Khalighi, H. Akhouayri, and S. Hranilovic, "Silicon-photomultiplier-based underwater wireless optical communication using pulse-amplitude modulation," *IEEE J. Ocean. Eng.*, early access, Jul. 22, 2019, doi: 10.1109/JOE.2019.2923501.
[16] S. Cova, M. Ghioni, A. Lacaita, C. Samori, and F. Zappa, "Avalanche photodiodes and quenching circuits for single-photon detection," *Appl. Opt.*, vol. 35, no. 12, pp. 1956–1976, Apr. 1996.
[17] S. Huang, S. M. Patanwala, J. Kosman, R. K. Henderson, and M. Safari, "Optimal photon counting receiver for sub-dead-time signal transmission," *J. Lightw. Technol.*, vol. 38, no. 18, pp. 5225–5235, Jun. 9, 2020.
[18] H. Ouh, S. Sengupta, S. Bose, and M. L. Johnston, "Dual-mode, enhanced dynamic range CMOS optical sensor for biomedical applications," in *Proc. IEEE Biomed. Circuits Syst. Conf. (BioCAS)*, 2017, pp. 1–4.
[19] H. Ouh, B. Shen, and M. L. Johnston, "Combined in-pixel linear and single-photon avalanche diode operation with integrated biasing for wide-dynamic-range optical sensing," *IEEE J. Solid-State Circuits*, vol. 55, no. 2, pp. 392–403, Feb. 2020.
[20] S. Deng *et al.*, "High dynamic range photo-detection module using on-chip dual avalanche photodiodes," *IEEE Photon. Technol. Lett.*, vol. 31, no. 24, pp. 1940–1943, Nov. 2019.
[21] ON Semiconductor. *R-SERIES SIPM: Silicon Photomultiplier Sensors, R-Series (SiPM)*. Accessed: Sep. 7, 2020. [Online]. Available: https://www.onsemi.com/products/sensors/silicon-photomultipliers-sipm/r-series-sipm
[22] X. Ma and G.-S. Kuo, "Optical switching technology comparison: Optical MEMS vs. other technologies," *IEEE Commun. Mag.*, vol. 41, no. 11, pp. S16–S23, May 2003.
[23] Hamamatsu. *MEMS Mirrors*. Accessed: Sep. 7, 2020. [Online]. Available: https://www.hamamatsu.com
[24] Y. Q. Lu, F. Du, Y.-H. Lin, and S.-T. Wu, "Variable optical attenuator based on polymer stabilized twisted nematic liquid crystal," *Opt. Exp.*, vol. 12, no. 7, pp. 1221–1227, Apr. 2004.
[25] Thorlab. *LCC1620 Liquid Crystal Shutter*. Accessed: Sep. 7, 2020. [Online]. Available: https://www.thorlabs.com
[26] E. Nicolescu, C. Mao, A. Fardad, and M. Escuti, "Polarization-insensitive variable optical attenuator and wavelength blocker using liquid crystal polarization gratings," *J. Lightw. Technol.*, vol. 28, no. 21, pp. 3121–3127, Nov. 23, 2010.
[27] I. I. Kim, B. McArthur, and E. J. Korevaar, "Comparison of laser beam propagation at 785 nm and 1550 nm in fog and haze for optical wireless communications," in *Proc. Opt. Wireless Commun. III*, vol. 4214, 2001, pp. 26–37.
[28] M. Ijaz, Z. Ghassemlooy, J. Pesek, O. Fiser, H. L. Minh, and E. Bentley, "Modeling of fog and smoke attenuation in free space optical communications link under controlled laboratory conditions," *J. Lightw. Technol.*, vol. 31, no. 11, pp. 1720–1726, Apr. 12, 2013.
[29] B. He and R. Schober, "Bit-interleaved coded modulation for hybrid RF/FSO systems," *IEEE Trans. Commun.*, vol. 57, no. 12, pp. 3753–3763, Dec. 2009.
[30] Spectral Sciences Inc. *MODTRAN*. Accessed: Sep. 7, 2020. [Online]. Available: http://modtran.spectral.com/
[31] R. N. Mahalati and J. M. Kahn, "Effect of fog on free-space optical links employing imaging receivers," *Opt. Exp.*, vol. 20, no. 2, pp. 1649–1661, Jan. 2012.
[32] J. M. Kahn and J. R. Barry, "Wireless infrared communications," *Proc. IEEE*, vol. 85, no. 2, pp. 265–298, 1997.
[33] M. A. Esmail, H. Fathallah, and M. Alouini, "Outdoor FSO communications under fog: Attenuation modeling and performance evaluation," *IEEE Photon. J.*, vol. 8, no. 4, pp. 1–22, Aug. 2016.
[34] A. Eisele *et al.*, "185 MHz count rate 139 dB dynamic range single-photon avalanche diode with active quenching circuit in 130 nm CMOS technology," in *Proc. Int. Image Sensor Workshop*, 2011, pp. 278–280.
[35] T. Hamza and M. A. Khalighi, "On limitations of using silicon photo-multipliers for underwater wireless optical communications," in *Proc. 2nd West Asian Colloquium Opt. Wireless Commun. (WACOWC)*, 2019, pp. 74–79.
[36] Y. Li, M. Safari, R. Henderson, and H. Haas, "Nonlinear distortion in SPAD-based optical OFDM systems," in *Proc. IEEE Globecom Workshops (GC Wkshps)*, Dec. 2015, pp. 1–6.
[37] E. Sarbazi, M. Safari, and H. Haas, "Photon detection characteristics and error performance of SPAD array optical receivers," in *Proc. 4th Int. Workshop Opt. Wireless Commun. (IWOW)*, 2015, pp. 132–136.
[38] S. M. Patanwala, I. Gyongy, N. A. Dutton, B. R. Rae, and R. K. Henderson, "A reconfigurable 40 nm CMOS spad array for lidar receiver validation," in *Proc. Int. Image Sensor Workshop (IISW)*, Jun. 2019, pp. 1–4.
[39] New Focus. *High-Speed Photoreceivers Models 1601*. Accessed: Sep. 7, 2020. [Online]. Available: https://www.newport.com/f/1-ghz-optical-receivers
[40] T. Plank, E. Leitgeb, P. Pezzei, and Z. Ghassemlooy, "Wavelength-selection for high data rate free space optics (FSO) in next generation wireless communications," in *Proc. 17th Eur. Conf. Netw. Opt. Commun.*, 2012, pp. 1–5.

SHENJIE HUANG (Member, IEEE) received the B.Sc. degree in optoelectronic engineering from Jiangnan University, Wuxi, China, in 2013, the M.Sc. degree in signal processing and communications and the Ph.D. degree in electrical engineering from the University of Edinburgh, Edinburgh, U.K., in 2014 and 2018, respectively, where he is currently a Research Associate with the Institute for Digital Communications. His main research interest is in free-space optical communications.

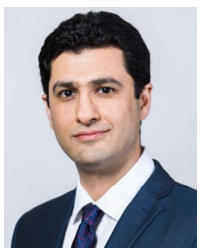

MAJID SAFARI (Member, IEEE) received the B.Sc. degree in electrical and computer engineering from the University of Tehran, Tehran, Iran, in 2003, the M.Sc. degree in electrical engineering from the Sharif University of Technology, Tehran, in 2005, and the Ph.D. degree in electrical and computer engineering from the University of Waterloo, Waterloo, ON, Canada, in 2011.

He is currently a Reader (Associate Professor) with the Institute for Digital Communications, University of Edinburgh, Edinburgh, U.K. Before joining Edinburgh in 2013, he held Postdoctoral Fellowship with McMaster University, Canada. His main research interests are the application of information theory and signal processing in optical communications, including fiber-optic communication, free-space optical communication, visible light communication, and quantum communication. He is currently an Associate Editor for the IEEE TRANSACTIONS ON COMMUNICATIONS and was the TPC Co-Chair for the 4th International Workshop on Optical Wireless Communication in 2015.